# INFLUENCE OF SMALL SPATIAL PERTURBATIONS OF SUPERSONIC FLOW VELOCITY ON THE HEAT FLUX TO THE CYLINDER SURFACE

Egorov I.V.
Central Aerohydrodynamic Institute, Zhukovsky,
Moscow region, Russia

### **Abstract**

The present paper deals with the three-dimensional flow in a shock layer at supersonic transverse flow conditions over the front surface of a cylinder under small, spatially-periodic perturbations along the transverse coordinate. Based on the numerical solution of the unsteady three-dimensional Navier-Stokes equations, it is shown that small imposed perturbations of the free stream velocity (0.5 - 3 %) along the transverse coordinate lead to the shock curvature and cause the formation of vortex structures in the shock layer and significant perturbations of the heat flux on the surface.

#### 1 Introduction

The problem of the influence of small perturbations on the heat transfer in hypersonic flow past blunt bodies is of great theoretical and practical interest. Particularly, in wind tunnel tests there are free-stream perturbations of various nature and intensity which can affect the measured characteristics.

Results of experimental investigations of the flow structure on the cylinder front surface at Mach numbers M=3, 5 and 6 were presented by Lapina & Bashkin [1], Bae S. et al. [2], where the spatial periodicity of limiting streamlines and heat-flux distribution along the transverse coordinate were demonstrated. The amplitude of the oscillations in the heat-flux distribution reached more than 25%. In paper [3] was suggested the following mechanism of this phenomenon. When the curved shock wave generates a vortex flow, the vortex remains (because of almost constant its

dissipation) and maintains the shock curvature. The computations [3] showed that the formation of an essentially three-dimensional flow with an internal vortex structure is possible. It was attempted in [4] to verify this hypothesis experimentally by introducing controlled perturbations in the free stream. However, these experiments showed that even after removal of the imposed free stream perturbations (up to the level of 50%), the flow returns to its twodimensional shape. Further computational and theoretical studies of the spatial structures in front of blunted bodies were performed [4] at free stream Mach number M=8 and Reynolds number Re  $\sim 10^4$ . Numerical studies [5] showed that small transversal perturbations on the free stream velocity (0.5-3 %) can lead to the shock curvature and formation of the periodic vortex structures that causes significant perturbations of the heat flux on the surface (more than 50%).

The present paper presents numerical simulations of the three-dimensional structures in the shock layer flow on the cylinder front surface (at M=6.1 and M=8, Re=3240,  $\gamma$ =1.4,  $T_w$ = $T_0$ /2, Pr=0.71) and on the sphere surface (at M=8, Re=5524,  $\gamma$ =1.4,  $T_w$ / $T_0$ =0.39, Pr=0.71). These structures are induced by small spatially-periodic perturbations along the transverse coordinate. The obtained numerical solutions help to explain the experimental results by [1] and [2] on the heat flux.

### 1.1 Equations and boundary conditions

Simulations of the three-dimensional flow over a blunted body are performed on the basis of numerical solutions of the Navier-Stokes equations. In an arbitrary curvilinear coordinate system  $\xi$ ,  $\eta$ ,  $\zeta$ , these equations are written in the divergence form

$$\frac{\partial \mathbf{Q}}{\partial t} + \frac{\partial \mathbf{E}}{\partial \xi} + \frac{\partial \mathbf{G}}{\partial \eta} + \frac{\partial \mathbf{F}}{\partial \zeta} = 0$$

Here **Q** is a vector of conservative dependent variables; **E**, **G**, and **F** are vectors of the flows. Vectors **Q**, **E**, **G** and **F** are related to the corresponding vectors **Q**<sub>c</sub>, **E**<sub>c</sub>, **G**<sub>c</sub>, **F**<sub>c</sub> in the Cartesian coordinate system  $x=x(\xi,\eta,\zeta)$ ,  $y=y(\xi,\eta,\zeta)$ ,  $z=z(\xi,\eta,\zeta)$  as

 $\mathbf{Q}=\mathbf{J}\mathbf{Q}_{c}$ , where  $\mathbf{J}=\partial(x.v.z)/\partial(c)$ 

where  $J = \partial(x,y,z)/\partial(\xi,\eta,\zeta)$  is the Jacobian of transformation,

$$\mathbf{E} = J(\mathbf{E_c} \frac{\partial \xi}{\partial x} + \mathbf{G_c} \frac{\partial \xi}{\partial y} + \mathbf{F_c} \frac{\partial \xi}{\partial z})$$

$$\mathbf{G} = J(\mathbf{E_c} \frac{\partial \eta}{\partial x} + \mathbf{G_c} \frac{\partial \eta}{\partial y} + \mathbf{F_c} \frac{\partial \eta}{\partial z})$$

$$\mathbf{F} = J(\mathbf{E_c} \frac{\partial \zeta}{\partial x} + \mathbf{G_c} \frac{\partial \zeta}{\partial y} + \mathbf{F_c} \frac{\partial \zeta}{\partial z})$$

The Cartesian components of vectors  $\mathbf{Q}_c$ ,  $\mathbf{E}_c$ ,  $\mathbf{G}_c$  have the form

$$\mathbf{Q_{c}} = \begin{vmatrix} \rho \\ \rho u \\ \rho v \\ \rho w \\ \rho e \end{vmatrix}, \mathbf{E_{c}} = \begin{vmatrix} \rho u \\ \rho u^{2} + p + \tau_{xx} \\ \rho uv + \tau_{xy} \\ \rho uw + \tau_{xz} \\ \rho uH + I_{x} \end{vmatrix},$$

$$\mathbf{G}_{c} = \begin{vmatrix} \rho v \\ \rho uv + \tau_{xy} \\ \rho v^{2} + p + \tau_{yy} \\ \rho vw + \tau_{yz} \\ \rho vH + I_{y} \end{vmatrix}, \mathbf{F}_{c} = \begin{vmatrix} \rho w \\ \rho wu + \tau_{xz} \\ \rho wv + \tau_{yz} \\ \rho w^{2} + p + \tau_{zz} \\ \rho wH + I_{z} \end{vmatrix}$$

where  $\rho$  is density, u, v, w are the Cartesian components of velocity vector  $\mathbf{V}$ , p is pressure,  $c_{\rm p}$  and  $c_{\rm v}$  are specific heats at constant pressure and volume,  $e=\rho(c_{\rm v}T+(u^2+v^2+w^2)/2)$  is the total energy per unit volume,  $H=c_{\rm p}T+(u^2+v^2+w^2)/2$  is the total enthalpy,  $\lambda$  is heat conductivity,  $\mu$  is dynamic viscosity, and  $\tau=-\mu\mathbf{s}$  is the viscousstress tensor:

$$\mathbf{s}_{xx} = 2\frac{\partial u}{\partial x} - \frac{2}{3}\operatorname{div}\mathbf{V}, \ \mathbf{s}_{yy} = 2\frac{\partial v}{\partial y} - \frac{2}{3}\operatorname{div}\mathbf{V},$$

$$\mathbf{s}_{zz} = 2\frac{\partial w}{\partial z} - \frac{2}{3}\operatorname{div}\mathbf{V}, \ \mathbf{s}_{xy} = \frac{\partial u}{\partial y} + \frac{\partial v}{\partial x},$$

$$\mathbf{s}_{xz} = \frac{\partial u}{\partial z} + \frac{\partial w}{\partial x}, \ \mathbf{s}_{yz} = \frac{\partial v}{\partial z} + \frac{\partial w}{\partial y};$$

 $\mathbf{q} = -\lambda \operatorname{grad}(T)$  is the heat flux vector.

The system of equations is closed by the perfect gas equation of state  $p = \rho R_G T/m$ . Here  $R_G$  is the universal gas constant; m is the gas molar weight. The dynamic viscosity varies with temperature in accordance with Sutherland's law; and the Prandtl number is assumed to be constant,  $Pr = \mu c_p/\lambda$ .

Computations are carried out using the dimensionless variables:  $x = \overline{x}R$ ,  $y = \overline{y}R$ ,  $z = \overline{z}R$ ,  $u = \overline{u}u_{\infty}$ ,  $v = \overline{v}u_{\infty}$ ,  $w = \overline{w}u_{\infty}$ ,  $t = \overline{t}R/u_{\infty}$ ,  $\rho = \overline{\rho}\rho_{\infty}$ ,  $p = \overline{p}(\rho_{\infty}V_{\infty}^2)$ ,  $T = \overline{T}T_{\infty}$ ,  $\mu = \overline{\mu}\mu_{\infty}$ ,  $p_{\infty} = 1/\gamma M_{\infty}^2$ , Reynolds number  $Re_{\infty} = \rho_{\infty}u_{\infty}R/\mu_{\infty}$ , where R is the radius of cylindrical blunt body or sphere.

### 1.2 Equations and boundary conditions

The initial boundary-value problem is solved numerically using the time-relaxation method on the basis of the integro-interpolation finite volume method. The difference analogues of the conservation laws are written as

$$\begin{split} & \frac{\mathbf{Q}_{i,j,k}^{n+1} - \mathbf{Q}_{i,j,k}^{n}}{\tau_{i,j,k}} + \frac{\mathbf{E}_{i+\frac{1}{2},j,k}^{n+1} - \mathbf{E}_{i-\frac{1}{2},j,k}^{n+1}}{h_{\xi}} + \frac{\mathbf{G}_{i,j+\frac{1}{2},k}^{n+1} - \mathbf{G}_{i,j-\frac{1}{2},k}^{n+1}}{h_{\eta}} \\ & + \frac{\mathbf{F}_{i,j,k+\frac{1}{2}}^{n+1} - \mathbf{F}_{i,j,k-\frac{1}{2}}^{n+1}}{h_{c}} = 0 \end{split}$$

where n – number of the time layer;  $\tau_{i,j,k}$  – time step size defined by the formula

$$\tau_{i,j,k} = \tau_o(a_{\min} + (a_{\max} - a_{\min}) \times \frac{J_{i,j,k} - \min(J_{i,j,k})}{\max(J_{i,j,k}) - \min(J_{i,j,k})},$$

where  $\tau_0$  – time step size corresponding to the cell of the maximum volume at given values of the parameters  $a_{\min}$  and  $a_{\max}$  (e.g.  $a_{\min} = 0.02$  and  $a_{\max} = 1$ ); i, j, k and  $h_{\xi}$ ,  $h_{\eta}$ ,  $h_{\zeta}$  – node numbers and steps for the coordinates  $\xi$ ,  $\eta$ ,  $\zeta$ ,

correspondingly. The usage of the spacevariable time step proportional to the volume of a unit cell, allows for considerable acceleration (approximately in order of magnitude) in obtaining of steady solutions by time-relaxation method.

the monotone difference scheme, For calculations of fluxes in half-integer nodes are carried out using the Riemann problem solution. Mathematically this problem comes to the solution of nonlinear set of algebraic equations. An approximate method of the problem solution is representation of Jacobian matrix  $\mathbf{A} = \partial \mathbf{E}/\partial \mathbf{Q}$ as  $A = R\Lambda R^{-1}$ , where  $\Lambda$  - diagonal matrix, elements of which are eigen values of the operator A. To approximate the convection component of flux vectors E, G, F in halfinteger nodes, The Godunov-type monotone scheme [6], [7] and the approximate Roe method [8] for the Riemann problem solution are used. Because the vectors E, G, F have similar forms, we consider in detail the E vector only. For this vector we have

$$E_{i+\frac{1}{2}} = \frac{1}{2} (E(Q_L) + E(Q_R) - R(Q_{LR}) \times$$

$$\times \Phi(\varphi(\lambda_i))R(Q_{LR})^{-1}(Q_R-Q_L))$$

where  $\Phi(\varphi(\lambda_i))$  – diagonal matrix with elements  $\varphi(\lambda_i)$ ,  $\lambda_i$  – eigen values of the operator

 $A = \partial E/\partial Q$ ;  $R_{LR} = R(Q_{LR})$  – matrix, columns of which are the right eigen vectors of the operator A.

For calculations of the eigen values and eigen vectors of operator  $\mathbf{A}$ , the method of approximate Riemann problem solution is used [8].  $\mathbf{\Phi}$  ( $\varphi$  ( $\lambda_i$ )),  $\mathbf{R}_{LR}$ ,  $\mathbf{R}_{LR}^{-1}$  are determined using the values of dependent variables

$$u_{LR} = \frac{u_L \sqrt{\rho_L} + u_R \sqrt{\rho_R}}{\sqrt{\rho_L} + \sqrt{\rho_R}},$$

$$v_{LR} = \frac{v_L \sqrt{\rho_L} + v_R \sqrt{\rho_R}}{\sqrt{\rho_L} + \sqrt{\rho_R}},$$

$$w_{LR} = \frac{w_L \sqrt{\rho_L} + w_R \sqrt{\rho_R}}{\sqrt{\rho_L} + \sqrt{\rho_R}},$$

$$H_{LR} = \frac{H_L \sqrt{\rho_L} + H_R \sqrt{\rho_R}}{\sqrt{\rho_L} + \sqrt{\rho_R}},$$

$$a_{LR}^2 = (\gamma - 1)(H_{LR} - \frac{1}{2}(u_{LR}^2 + v_{LR}^2 + w_{LR}^2))$$

where a – is the local speed of sound.

To fulfill the entropy condition for numerical solutions, the function  $\varphi(\lambda_i)$  is specified as

$$\varphi(\lambda) = \begin{cases} |\lambda|, & |\lambda| > \varepsilon \\ \frac{\lambda^2 + \varepsilon^2}{2\varepsilon}, & |\lambda| \le \varepsilon \end{cases}$$

where  $\varepsilon$  - parameter responsible for dissipative characteristics of the difference scheme. (typically  $\varepsilon = 10^{-3}$ ).

To increase the approximation to the second order, in the interpolation of dependent variables on the unit cell edges, the principle of minimum derivatives (MUSCL) is used [9-11]

$$\mathbf{Q}_{L} = \mathbf{Q}_{i} + \frac{1}{2} m(\mathbf{Q}_{i} - \mathbf{Q}_{i-1}, \mathbf{Q}_{i+1} - \mathbf{Q}_{i}),$$

$$\mathbf{Q}_{R} = \mathbf{Q}_{i} - \frac{1}{2} m(\mathbf{Q}_{i+1} - \mathbf{Q}_{i}, \mathbf{Q}_{i+2} - \mathbf{Q}_{i+1})$$

and the function m(a,b) is taken in the form

$$m(a,b) = \begin{cases} a, & ab > 0, & |a| < |b| \\ b, & ab > 0, & |a| > |b| \\ 0, & ab \le 0 \end{cases}$$

In approximation of the diffusive component of flux vectors **E**, **G** and **F** on the unit cell edges, the second-order central difference scheme is employed. Calculations of derivatives are carried out using the formulas

$$\frac{\partial \mathbf{U}}{\partial \xi}_{i+\frac{1}{2},j,k} = \frac{\mathbf{U}_{i+1,j,k} - \mathbf{U}_{i,j,k}}{h_{\xi}},$$

$$\frac{\partial \mathbf{U}}{\partial \eta}_{i+\frac{1}{2},j,k} = \frac{1}{4h_{\eta}} (\mathbf{U}_{i+1,j+1,k} + \mathbf{U}_{i,j+1,k} - \mathbf{U}_{i+1,j-1,k} - \mathbf{U}_{i,j-1,k})$$

$$\frac{\partial \mathbf{U}}{\partial \zeta}_{i+\frac{1}{2},j,k} = \frac{1}{4h_{\zeta}} (\mathbf{U}_{i+1,j,k+1} + \mathbf{U}_{i,j,k+1} - \mathbf{U}_{i+1,j,k-1} - \mathbf{U}_{i,j,k-1})$$

here U – is the vector of non-conservative dependent variables. The difference scheme stencil, on which the full Navier-Stokes or Reynolds equations are approximated, consists of 25 points. It seems that the foregoing implicit nonlinear difference scheme is unconditionally stable for the linear problem.

### 1.3 Solution of nonlinear finite-difference equations

The difference approximation of Section 1.2 and the boundary conditions lead to the nonlinear system of algebraic equations  $\mathbf{F}(\mathbf{X}) = 0$ , where  $\mathbf{X}$  – vector of the discrete variables (nodal values of gas-dynamic variables, including boundary nodes of the computational grid). The problem is effectively solved using the well-known Newton iterative method, the main advantage of which is a quadratic convergence rate. The system  $\mathbf{F}(\mathbf{X}) = 0$  is solved using the modified Newton method

$$\mathbf{X}^{[k+1]} = \mathbf{X}^{[k]} - \tau_{k+1} D_{k_o}^{-1} \mathbf{F}(\mathbf{X}^k),$$

where  $\mathbf{D}_{ko} = (\partial \mathbf{F}/\partial \mathbf{X})_{ko}$  - Jacobian matrix, k,  $k_o$  - iteration numbers,  $k_o \leq k$ . The regularization parameter of Newton method relative to the initial approximation  $\tau_k$  is determined using the formula [12]

$$\tau_{k+1} = \frac{(\Delta \mathbf{X}^{[k]} - \Delta \mathbf{X}^{[k-1]}, \mathbf{X}^{[k]} - \mathbf{X}^{[k-1]})}{(\Delta \mathbf{X}^{[k]} - \Delta \mathbf{X}^{[k-1]})^2},$$

where  $\Delta X^{[k]}$  - correction vector. As the iteration process convergence  $\tau_k \to 1$ , and the convergence rate theoretically tends to the quadratic one.

The most time-consuming parts of the Newton method algorithm are generation of the matrix  $\mathbf{D_k} = \partial \mathbf{F}/\partial \mathbf{X_k}$  and computations of a solution to this matrix. Because related approximation for each computational grid contains only few neighboring nodes (in threedimensional case 25 for TVD scheme), the laboriousness of Jacobian matrix generation is O(N), where N – the number of nodes for the finite difference problem. The Jacobian matrix generated using the finite difference procedure of the residual vector on the vector of desired mesh variables. Application of the finite difference method to generation of the Jacobian matrix is based on long-term investigations on numerical simulation of gas-dynamic problems. For example, a similar procedure is used in [13] for solutions of the initial-boundary problems on adaptive grids.

RAM memory space and CPU time, which are required for solving the linear system of algebraic equations on iteration for nonlinearity

$$(\partial \mathbf{F}/\partial \mathbf{X})_{k} \Delta \mathbf{X}^{[k]} = -\mathbf{F}(\mathbf{X}^{[k]}),$$

considerably depends on the degree of matrix  $(\partial F/\partial X)$ sparseness. For Navier-Stokes equations approximation using the foregoing second-order difference scheme, the operator  $\partial F/\partial X_k$  has sparse block 25-diagonal structure. and its elementary block is a full matrix of size 5×5. Solutions of the linear system of algebraic equations related to each iteration of the nonlinear problem, are carried out using the direct [14] and iterative [15] methods. These techniques were repeatedly tested in numerical experiments and prove their reliability and high efficiency.

### 2 Boundary conditions and computational grid

The origin of Cartesian coordinate system x = y = 0 for the two-dimensional computational domain coincides with the center of circle, while the cylinder surface for x < 0 is located at a distance R = 1. For x > 0, this surface is flat and has the length L = 0.3.

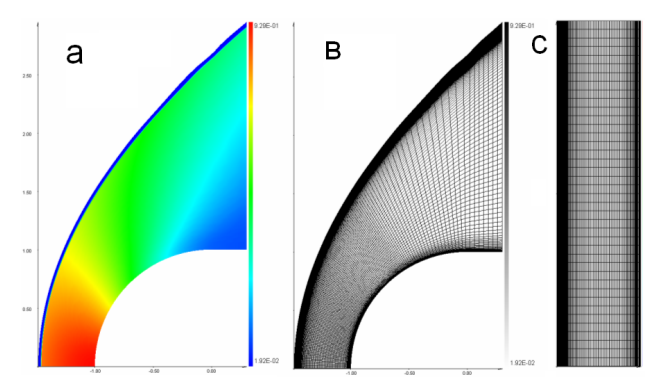


Figure 1. Pressure field (a) and the computational grid with clustering in the x-y plane (b) and in the x-z plane (c), M = 6.1,  $T_w = 0.1$ , Re = 3240.

The inflow boundary of the two-dimensional computational domain is located in the undisturbed free-stream with the parameters  $u_{\infty}=1$ ,  $v_{\infty}=0$ ,  $T_{\infty}=1$ ,  $P_{\infty}=1/\gamma M^2$ . On the body surface, the velocity is u=v=0 and temperature is  $T=T_W/T_0$ , where  $T_0/T_{\infty}=1+0.5(\gamma-1)M^2$ . The symmetry conditions are imposed on the axis y=0 (v=0,  $\partial F/\partial \xi=0$ , F=u,P,T). On the outflow boundary, the 'soft' boundary conditions are imposed as  $\partial F/\partial \xi=0$ , F=u,v,P,T ( $\xi$  is the normal to the right boundary). In test calculations for

the computational domains related to L=0.3-1, the scheme was verified by means of removing few grid lines near the outflow boundary. It was found that the length L=0.3 was sufficient to avoid any influence of the outflow boundary conditions on the flow field for x<0. The two-dimensional computational grid has  $N_{\eta}$ =151 nodes along the normal and  $N_{\xi}$ =111 along the body surface.

In the three-dimensional case, one spanwise period of sinusoidal velocity perturbations  $u_{\infty}=1+A\cdot\sin(2\cdot\pi z/\lambda)$  with the amplitude A=0-0.03 and period  $\lambda=\Delta Z/R=0.1\div10$  ( $\Delta Z$  is the computational domain size in z-coordinate) was imposed on the free-stream velocity field

The three-dimensional computational grid with  $151\times111\times122$  nodes was constructed by a uniform duplication of the two-dimensional grid in z-direction. The periodic boundary condition is imposed in this direction. Namely, the values of the dependent variables of the problem of the left (right) end were equated with their values in the last but one right (left) node of the field. Let us note that such a boundary condition contained, as a particular case, the boundary condition of the two-dimensional flow implementation ( $\partial F/\partial z=0$ ).

As the Reynolds number increases, the boundary layer thickness and the near shock layer thickness decrease and, consequently, the number of nodes in the near shock layer also decreases (Fig. 2). Therefore, the grid clustering just behind the shock wave is performed, in addition to the near-wall clustering, in order to improve the resolution in the near shock layer.

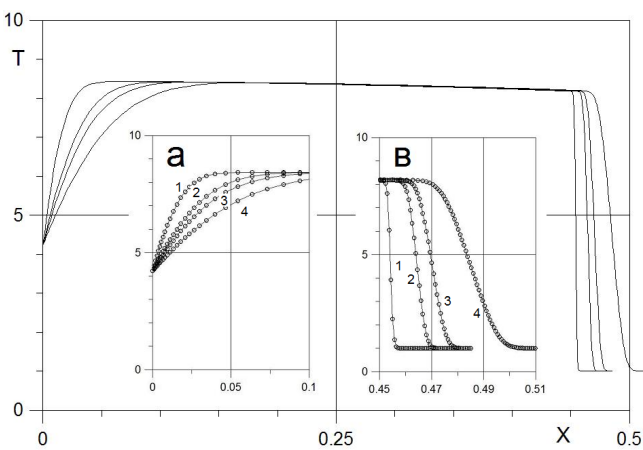
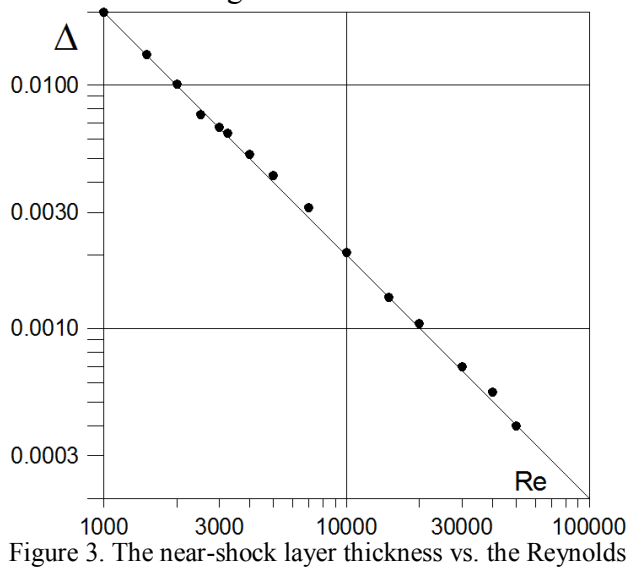


Figure 2. Temperature distributions over axis y=0 in the near-wall boundary layer (a) and in the near-shock layer

(b) for M=6.1, 
$$T_w$$
=0.1 (1 – Re= $10^4$ , 2 - Re= $3 \times 10^3$ , 3 - Re= $2 \times 10^3$ , 4 - Re= $10^3$ ).

Figure 3 shows that the near-shock layer thickness  $\Delta_{ShW}$ , obtained numerically, is inversely proportional to the Reynolds number. For the conservation of grid resolution in  $\eta$ -coordinate (normal to the rigid boundary), it is necessary to increase the number of nodes in the near-shock layer proportionally to the Reynolds number. In particular, only one computational cell falls into the near-shock layer in the case of uniform grid with number of nodes  $N_{\eta}\sim 100$ , whereas 10-30 nodes fall into this layer in the case of clustered grid.



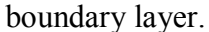
number.

The foregoing clustering is necessary to obtain a reliable solution in the three-dimensional case, because the shock wave stand-off distance significantly varies versus the z-coordinate.

## 3 Boundary conditions and computational grid Small spatial perturbations of flow over a cylinder

The problem of a supersonic gas flow over a cylindrical blunt body was solved (Fig. 4) under imposed spanwise periodic perturbations of the free stream velocity  $u_{\infty}=1+A\cdot\sin(2\cdot\pi z/\lambda)$ . The free-stream parameters were taken from [3]: Re=3240, M=6.1, Prandtl number Pr=0.71, the wall temperature  $T_w=0.5T_0$  (where  $T_0$  is the stagnation temperature), specific heat ratio  $\gamma=1.4$ . Sutherland's law was used for the viscosity law.

Figure 5 shows the pressure and temperature distributions in the boundary layer and in the near-shock layer for different values of the freestream velocity  $u_{\infty}$  (from 0.94 to 1.06). These distributions were obtained using the twodimensional calculations. The normalized pressure distributions  $p=(p-p_{min})/(p_{max}-p_{min})$  and temperature distributions  $T=(T-T_{min})/(T_{max}-T_{min})$ are collapsed to one curve, as shown in Fig. 6a. It is seen from Fig. 6b, that a small free stream velocity perturbation  $\Delta u_{\infty}$  leads to doubling of the temperature and pressure disturbances in the



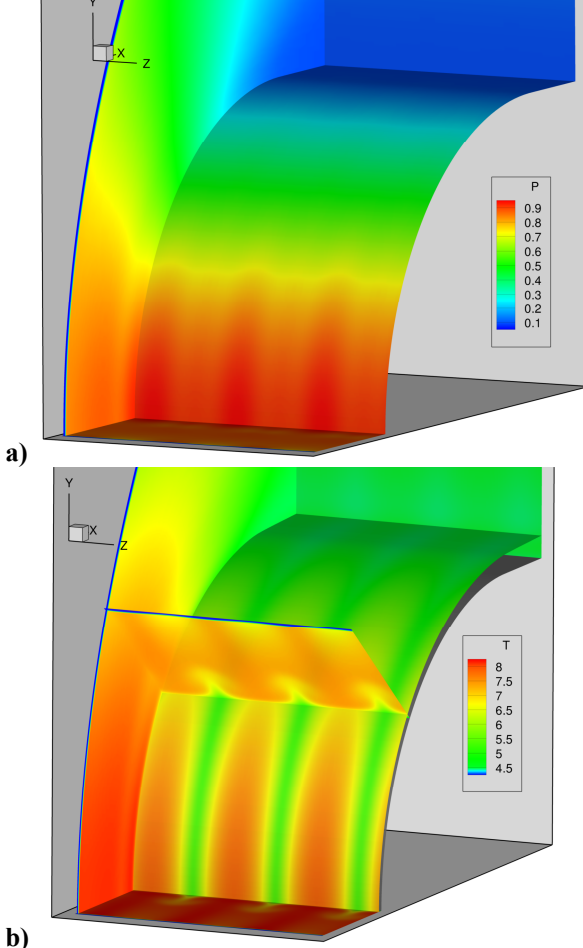


Figure 4. Pressure distribution (a) and temperature distribution (b) on the cylinder front surface in the case of imposed spanwise perturbations of free stream velocity  $u_{\infty}=1+A\cdot\sin(2\cdot\pi z/R)$  with amplitude A=0.03 and period  $\lambda = \Delta Z/R = 0.3$ .

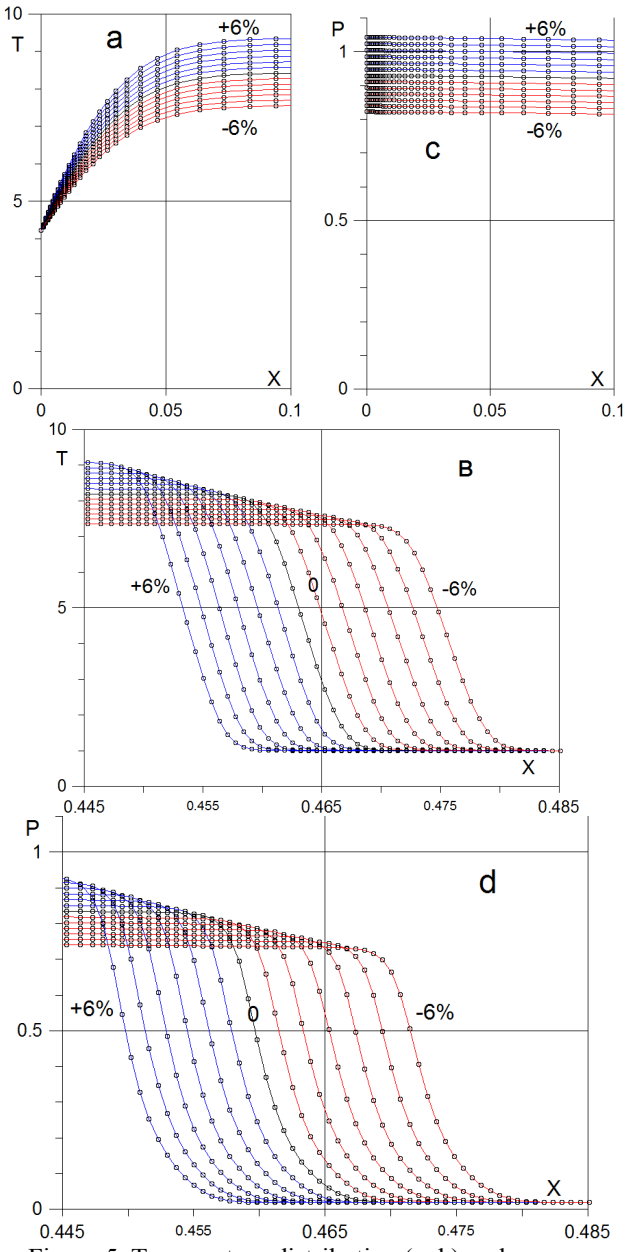


Figure 5. Temperature distribution (a, b) and pressure distribution (c, d) along the axis y=0 in the boundary layer (a, c) and in the near-shock layer (b, d) at different values of the free-stream velocity  $u_{\infty}+\Delta u_{\infty}$ ,  $\Delta u_{\infty}/u_{\infty}=-6,-5,-4,-3,-$ 2,1,0,1,2,3,4,5,6%.

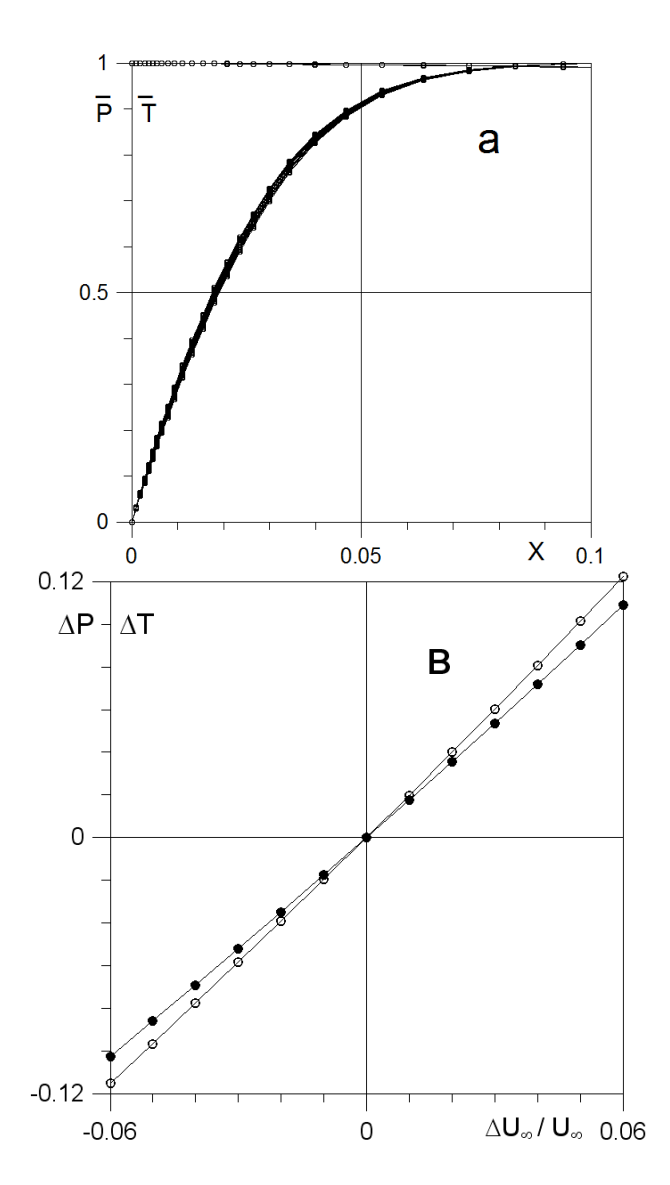


Figure 6. The normalized distributions of pressure and temperature (a) along the axis y=0, and variations of normalized  $\Delta P$ ,  $\Delta T$  (b) as functions of the free-stream velocity variation  $\Delta u_{\infty}/u_{\infty} = \pm 6\%$ .

Figure 7 shows the shock wave fronts for various periods of the imposed perturbations  $\lambda = \Delta Z/R = 0.1 \div 10$  with amplitude A=0.03. For small  $\lambda$ , the shock wave is close to its undisturbed two-dimensional shape (2D). As  $\lambda$ increases, the shock shape tends to quasi-three-(2D-3D).dimensional The quasi-threedimensional (2D-3D) flow is obtained as a composition of the results of two-dimensional calculations for the values of free stream velocity  $u_{\infty}=1+A\cdot\sin(2\cdot\pi z/\lambda)$ . The maximum stand-off distance of the shock is reached at  $\lambda$ = 0.7.

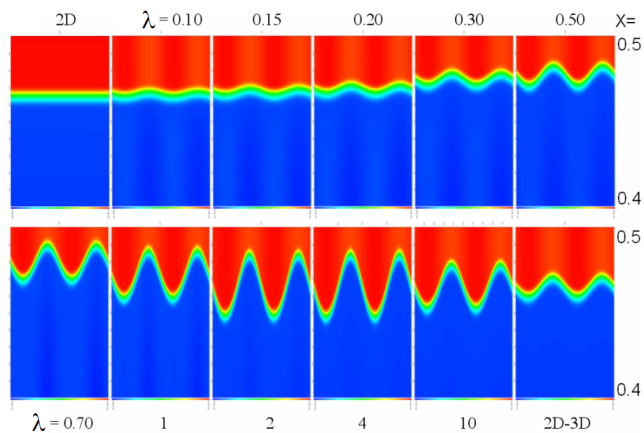
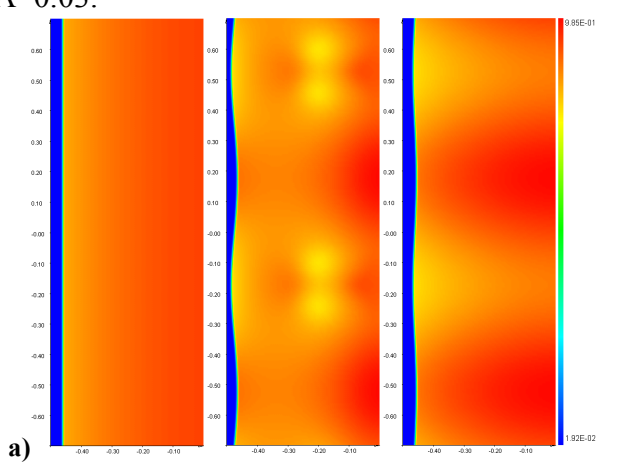


Figure 7. The shock wave front for various periods  $\lambda$ =0.1÷10, the imposed velocity amplitude A=0.03.

It is seen from the comparison of three types of pressure and temperature fields in the x-z plane (v=0) (two-dimensional without perturbations, three-dimensional ( $\lambda$ =0.7), and quasi-threedimensional flows) that the values of P and T in the three-dimensional case do not exceed the corresponding values in the quasi-threedimensional case (Figs. 8, 9a). Variations of the boundary layer thickness are also seen in the temperature field for the both three-dimensional quasi-three-dimensional cases. indicates the presence of maximum and minimum heat fluxes on the body surface with higher values than in the quasi-threedimensional case. A reverse subsonic threedimensional vortex flow is formed within the shock layer due to the pressure difference in different sections. This flow has maximum Mach number M $\approx$ 0.4 in the case of  $\lambda$ =0.7 at A=0.03.



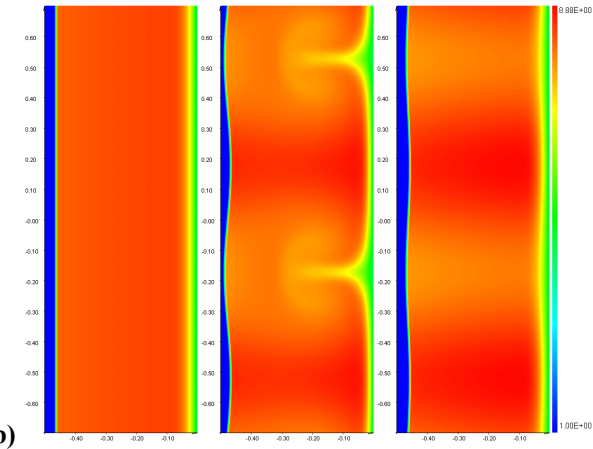


Figure 8. Pressure fields (a) and temperature fields (b) in x-z plane (y=0) at 3%-perturbations of the free-stream velocity for the two-dimensional, three-dimensional  $(\lambda=0.7)$ , and quasi-three-dimensional cases.

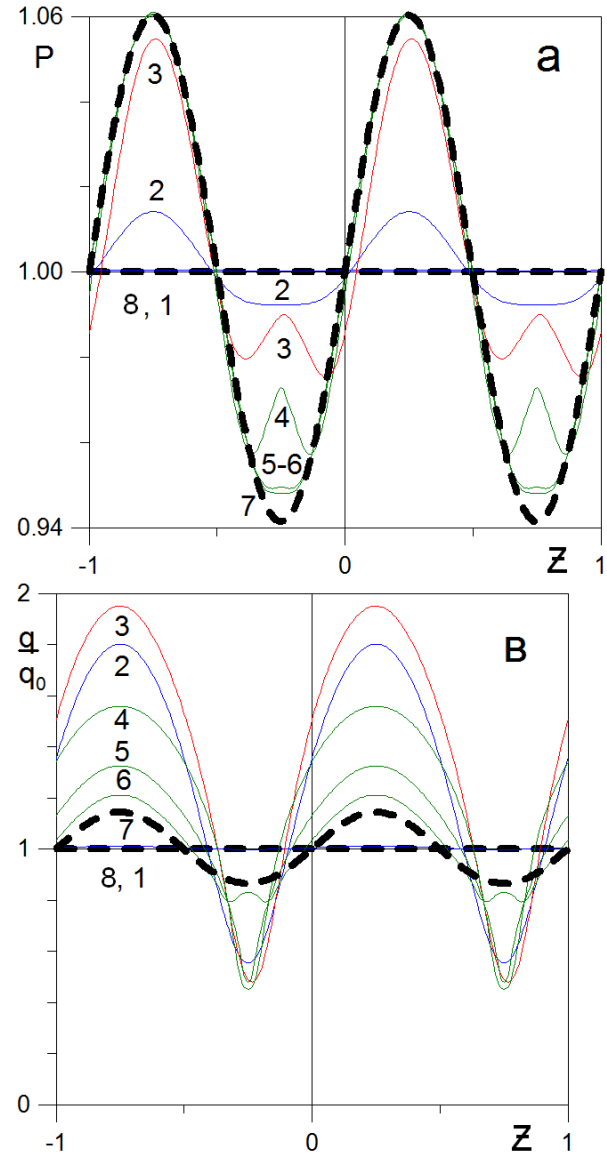


Figure 9. Pressure distribution (a) and normalized heat flux distribution (b) over the surface along the line x=y=0

at 3%-perturbations of the free-stream velocity. Curves 1-6 correspond to  $\lambda$ =0.1, 0.2, 0.5, 1, 2, 4; the dot line 8 corresponds to the two-dimensional case; curve 7 corresponds to the quasi-three-dimensional case.

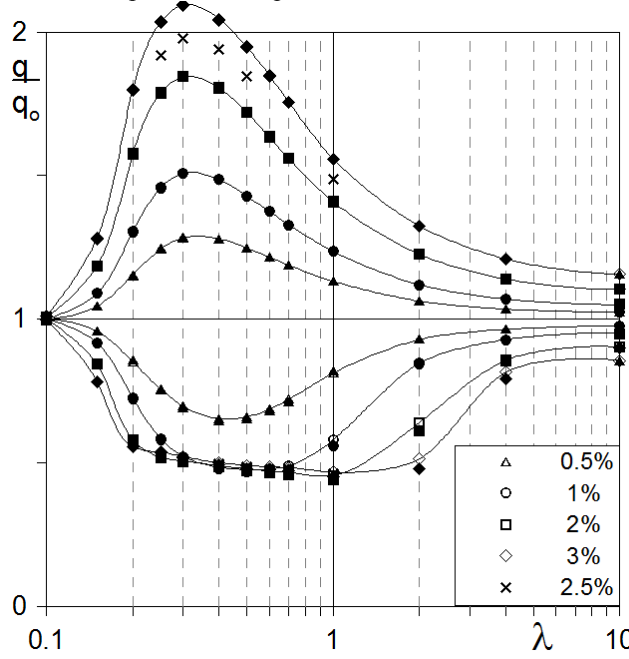


Figure 10. Normalized maximum and minimum heat fluxes (upper and lower branches) on the cylinder surface for M=6.1 (a) and M=8 (b) as functions of  $\lambda$ = $\Delta$ Z/R at the free stream velocity perturbation amplitudes A= 0.005, 0.01, 0.02, 0.03 for the grids 151×111×62 (light markers) and 151×111×122 (dark markers).

Figure 10 shows the maximum and minimum heat fluxes (normalized to their values in the two-dimensional case) versus the period  $\lambda$  of imposed perturbation period. These distributions reach their extreme values at  $\lambda=0.3$ . The velocity perturbation of 1% leads to the increase in heat flux by approximately 50%. The heat fluxes for small  $\lambda$  tend to 1 (their value for the two-dimensional case). The heat fluxes for high λ tend towards their values in the quasi-threedimensional case. Similar dependences were obtained for Mach number M=8 at Re=3240 and T<sub>w</sub>=0.39. The foregoing numerical solutions explain the experimental results on the heat flux measurements. It is important to note that the all three-dimensional solutions return to the solution for the two-dimensional case, if the considered herein small perturbations (A=1-3%) were switched off.

Because actual perturbations may have different spatial forms, it is interesting to compare the heat flux disturbances induced by the z-periodic perturbation  $u_{\infty}=1+A\cdot\sin(2\pi z/\lambda)$  and the y-

periodic perturbation  $u_{\infty}=1+A\cdot\sin(2\pi y/\lambda)$ 11). three-dimensional (Figure Since the for y-periodic perturbations equivalent to the two-dimensional problem, the heat fluxes in this case are obtained from the solution of two-dimensional problem. Figure 11 shows the dimensionless heat fluxes as functions of  $\lambda$  at Re=3240, A= -1\%, -0.5\%, 0.5% and 1%; the flow parameters are M=6.1,  $T_{w}/T_{0}=0.5$ and M=8.  $T_{\rm w}/T_0=0.39$ . comparison, the corresponding distributions for the z-periodic perturbations are shown by the dotted lines.

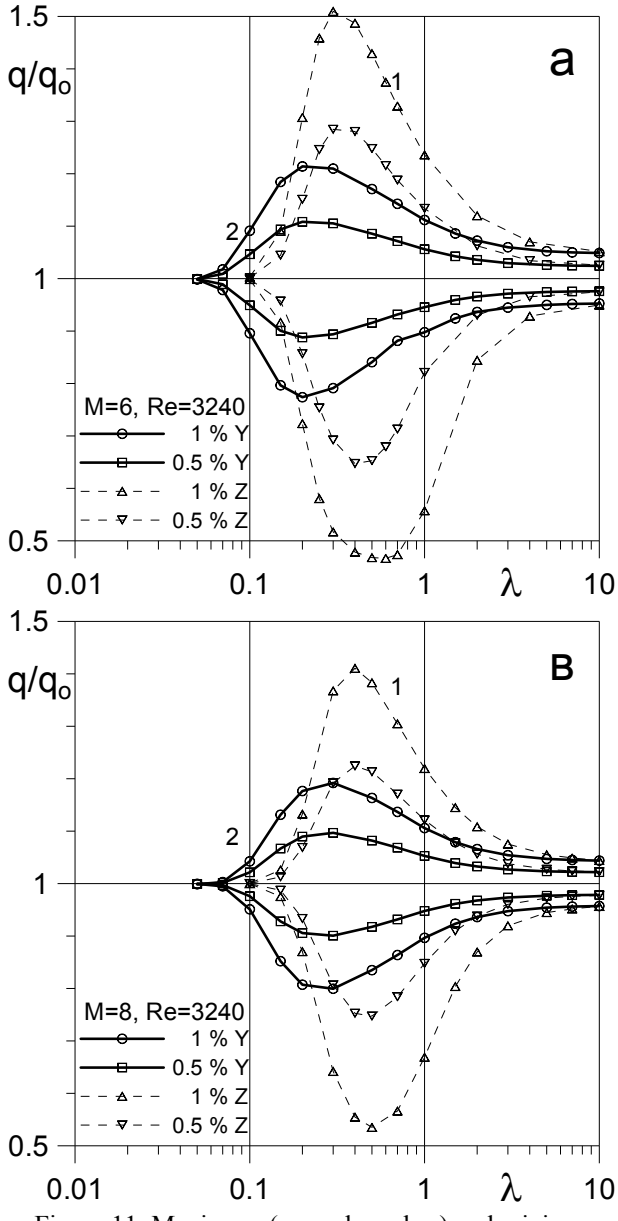


Figure 11. Maximum (upper branches) and minimum (lower branches) heat fluxes to the cylinder surface as functions of the period  $\lambda$  at Re=3240, (a) M=6.1,  $T_w/T_0$ =0.5 and (b) M=8,  $T_w/T_0$ =0.39. The dotted lines correspond to the z-periodic perturbations of amplitude

A=0.5% and A=1%, and the solid lines correspond to the y-periodic perturbations of the same amplitude.  $(q_0 - heat)$ flux without perturbations for the two-dimensional case). Small amplitudes of perturbations are chosen to avoid considerable influence on the main flow. It is seen that the heat flux disturbances induced by the z-periodic perturbations approximately two times larger than those induced by the vperiodic perturbations. As the amplitude of imposed perturbations decreases two times, the heat flux deviations cut in half. As compared to the case of z-periodic perturbations, the maximum heat flux induced by the y-periodic perturbations occurs at smaller values of the perturbation wavelength: λ<sub>m</sub>≈0.2 (M=6.1) and  $\lambda_m \approx 0.3$  (M=8). As  $\lambda$  decreases, the heat flux tends to the unperturbed level  $(u_{\infty}=1)$ . As  $\lambda$ increases, the heat flux approaches the value at corresponding values of free stream velocity  $(u_{\infty}=1+A).$ 

### **5 Conclusions**

A supersonic flow over a blunt cylinder under imposed spanwise-periodic free-stream velocity perturbations was investigated using numerical solutions of the Navier-Stokes equations.

It was shown that the computational grid in the near-shock layer significantly affects the numerical solution. On a sufficiently fine (versus the normal coordinate y) grid, three-dimensional solutions in the near-shock layer return to the two-dimensional form after switching off the imposed velocity perturbations of the level 1-3%. If the grid is not sufficiently fine, the induced three-dimensional structures do not vanish when the perturbation is switched off.

Numerical computations on sufficiently fine grids show that small ( $\sim$ 1%) spanwise-periodic perturbations of the free-stream velocity can lead to a significant ( $\sim$ 50%) increase of the heat flux to the cylinder surface. This effect is due to the three-dimensional structures formed in the shock layer where the flow is subsonic.

The level of heat-flux fluctuations depends on the period and amplitude of imposed threedimensional perturbations. High heat-flux fluctuations are observed at the spanwise period equal to 0.2÷0.7 of the cylinder radius. In particular, the heat flux maximum is reached at  $\lambda_m$ =0.3. For a perturbation period decrease, the value of the heat flux fluctuation amplitude reduces down to zero while when it increases, it tends towards the values obtained for the two-dimensional case at free-stream velocities corresponding to those periodically varying in the z-coordinate free stream.

As the perturbation period decreases  $(\lambda < \lambda_m)$ , the amplitude of heat-flux fluctuation reduces to zero. As  $\lambda$  increases  $(\lambda > \lambda_m)$ , the heat-flux amplitude tends to the value obtained for the two-dimensional case. The wall pressure distributions for different periods are bounded by the distributions corresponding to these two limiting cases.

It should be noted that for all cases considered, the spatial perturbations lead to appreciable changes of the heat flux, and there is a length-scale at which the heat-flux attains maximum and minimum levels. E.g., the y-perturbations of 0.5% induce approximately 10% fluctuations of the heat flux in the case of cylinder or sphere. The z-periodic fluctuations of the same level induce 20-25% fluctuations of the heat flux in the case of cylinder. At higher levels of the imposed perturbations, the induced heat-flux fluctuations grow proportionally. The spatial length scale, at which the heat-flux fluctuations are extreme, is approximately a half of the shock layer thickness at the critical point.

The foregoing results are consistent with the theoretical studies and help to explain the available experimental results [1-2].

The work has been carried out in Moscow Institute of Physics and Technology (MIPT) with the financial support of Russian Scientific Foundation (project No. 14-19-00821) and RFBR (project No. 14-08-00793)

### References

- [1] Lapina N.G. and Bashkin V.A., Experimental investigation of the flow pattern and heat transfer in the vicinity of the spreading line of a circular cylinder in a supersonic transverse flow with Mach numbers M=3, 5, and 6, Trudy TsAGI (TsAGI Proceedings), Issue 2203, pp 44 49, 1983 [in Russian].
- [2] Bae S., Lele S.K., Sung H.J., Influence of inflow disturbances on stagnation-region heat transfer,

- Journal heat transfer, Vol. 122, No. 2, pp 258-265, 2000
- [3] *Drozdov S.M.*, Vortex structure generation on the frontal surface of a cylinder set transversely in a hypersonic flow, *Fluid dynamics*, Vol. 41, No. 6, pp 857-870, 2006
- [4] *Drozdov S.M.*, Numerical modeling of three-dimensional vortex structures in hypersonic transverse flow past a cylinder, *Fluid dynamics*, Vol. 45, No. 5, pp 691-702, 2010
- [5] *Bashkin V.A., Egorov I.V.*, "Numerical simulation of viscous perfect gas flow", Moscow: Fizmatlit (in Russian) 2012. 372 p., 2012
- [6] Godunov S.K., A Difference Scheme for Numerical Solution of Discontinuous Solution of Hydrodynamic Equations, Math. Sbornik, No. 47, pp 271-306; translated US Joint Publ. Res. Service, JPRS 7226, 1959
- [7] Godunov S.K., Zabrodin A.V., Ivanov M.Ya., Kraiko A.N., Prokopov G.P.: Numerical solution of multidimensional problems of gas dynamics. Nauka, Moscow, 1976
- [8] Roe P.L., Approximate Riemann solvers, parameter vectors and difference scheme, *Journal computational physics*, v. 43, pp. 357-372, 1981
- [9] V.P. Kolgan. Application of the Principal of Minimum Derivatives to the construction of difference schemes for computing discontinuous solutions of gas dynamics (in Russian). *Uch. Zap.TsaGI, Russia,* 3(6):68-77, 1972
- [10] *Harten A.*, High resolution schemes for hyperbolic conservation laws // Journal Computational Physics. v. 49. pp. 357-372, 1983
- [11] Ivanov M.Ya., Krupa V.G., Nigmatullin R.Z. Implicit improved accuracy Godunov scheme for integrating the Navier-Stokes equations. Zh. Vychisl.Matematiki i Matem Fiziki, v.29, no.6, pp.888-901, 1989
- [12] Karimov T.Kh. On certain iterative methods for solving non-linear equations in Hilbert space, Dokl. Akad. Nauk USSR, v.269. no. 5. pp. 1038 – 1046, 1983
- [13] *Babikov P.E., Yegorov I.V.*, 1988. On one version of the adaptive grid generation to solve evolution problems // Proc. Soviet Union-Japan SCFD. Khabarovsk, v. 2. pp. 222 227, 1988
- [14] *Egorov I.V., Zaytsev O.L.,* On one approach to numerical solution of two-dimensional Navier-Stokes equations by shock-capturing method. Zh. Vychisl.Matematiki i Matem Fiziki. v. 31. no.2. pp. 286-299., 1991
- [15] Babaev I. Yu., Bashkin V.A., Egorov I.V. Numerical solution of Navier-Stokes equations using iterative methods of variative type. Zh. Vychisl.Matematiki i Matem Fiziki, v. 34. no.11. pp. 1693-1703, 1994

### **Copyright Statement**

The authors confirm that they, and/or their company or organization, hold copyright on all of the original material

### INFLUENCE OF SMALL SPATIAL PERTURBATIONS OF SUPERSONIC FLOW VELOCITY ON THE HEAT FLUX TO THE CYLINDER SURFACE

included in this paper. The authors also confirm that they have obtained permission, from the copyright holder of any third party material included in this paper, to publish it as part of their paper. The authors confirm that they give permission, or have obtained permission from the copyright holder of this paper, for the publication and distribution of this paper as part of the ICAS 2014 proceedings or as individual off-prints from the proceedings.